TP02: On Bose–Einstein condensates with spatially inhomogenous scattering length

Candidate Number: 468823 Supervisor: Dr Mason Porter
Wordcount: 6750 [1]

[1]Using TeXcount, http://app.uio.no/ifi/texcount/online.php

Abstract

I investigated a Bose–Einstein condensate confined harmonically to 1D, within the framework of Gross–Pitaevskii mean–field theory. I consider the 1D Gross–Pitaevskii equation with a combined step in its external potential and nonlinear terms. I generalise solitary wave solutions to the equation in its nonlinear limit, to take into account a constant potential and nonlinearity. I then generalise an effective potential theory to take into account the combined step. The theory allows us to predict the linear stability eigenvalues of the Bogoliubov–de Gennes equations. The theoretical work is supplemented by numerical investigations of the solitary wave solutions, mainly the effect of varying the step width on the solitary wave solutions. It is found that dark solitary waves are unstable for all step widths: either with positive imaginary eigenvalues; or with a complex eigenvalue quartet. Bright solitary waves undergo a pitchfork bifurcation from stability to instability (or vice–versa, depending on the sign of the step) as the step width alters. The size of the relevant eigenvalues are predicted well by the theory, becoming quantitatively less accurate as the step strength is increased, but maintaining their qualitative accuracy. Finally the time–development of an unstable solitary wave is shown. It is found that the solitary wave leaves the step region, emitting dispersive waves as it crosses the step edge. It is hoped that this work will contribute to ongoing investigations into Bose–Einstein condensates with spatially inhomogenous scattering length.

1 INTRODUCTION

Predicted theoretically by Bose and Einstein in 1924 [1, 2], a Bose–Einstein condensate (BEC) is a quantum phase entered by a gas of bosons below a critical temperature, T_c. Below this temperature, a quantum state of the system is macroscopically occupied. Following the theoretical suggestions of Bose and Einstein, it was a long time before BEC would be achieved experimentally. The first hints of the phenomena were in super–fluid ^{4}He [3], where the transition temperature was reasonably well predicted by an ideal Bose gas theory . However, the interactions in ^{4}He are very strong (due to high particle density), and thus an ideal Bose gas theory is not applicable. Another BEC-like phenomena is superconductivity, which, in the BCS theory, relies on Cooper pairs of electrons (which are bosons) forming a macroscopic coherent state [4].

The first true realisation of BEC was in ultra–cold atoms, due to Anderson *et al* in 1995 [5], with ^{87}Rb atoms. Since then BEC has been achieved in gases of ^{23}Na, ^{7}Li, ^{41}K, and ^{133}Cs atoms, amongst others [6, 7, 8, 9, 10, 11]. The atoms are first trapped in a magneto–optical trap before undergoing laser cooling. These cold atoms are then further cooled evaporatively (see [5] for further detail). At the temperatures involved, typically μK and below, the equilibrium phase is the solid state. To maintain the gaseous state a dilute gas is used. In a dilute gas, three-body collisions are very rare, the lifetime of the gaseous state is thus long enough to perform experiments [12].

The large inter-particle distances in dilute alkali gases lead to weak interactions. The theory of weakly interacting Bose gases, in the low temperature limit, is built around the Gross–Pitaevskii (GP) equation. The GP equation arises from a mean field treatment of the full many body theory, discussed in detail in section 2. Using a highly anisotropic harmonic trap, it is possible to produce a 'cigar' shaped, 1D condensate, which is described by the 1D GP equation:

$$i\frac{\partial}{\partial t}\psi(z,t)=\left(-\frac{1}{2}\frac{\partial^2}{\partial z^2}+V_{\rm ext}(z)+g(z)|\psi|^2\right)\psi(z,t). \quad (1)$$

The squared modulus of the *order–parameter*, $\psi(z,t)$, gives the atomic density. The second term on the right hand side is an external potential term, the third is a result of inter-atomic interactions. Both external potential and interactions are experimentally controllable. The external potential is implemented using magnetic or optical fields [18], the inter-atomic interactions are manipulated via Feshbach resonance management. Feshbach resonances can be exploited to tune the interactions to be attractive, repulsive, or zero, again, by application of a magnetic or optical field [20, 21].

In the case of $V_{\rm ext}=0$ and $g=\pm 1$ the GP equation is known as the non–linear Schrodinger

equation (NLS). Most weakly nonlinear, dispersive, energy-preserving systems can be described by the NLS in an appropriate limit [38]. The NLS is, therefore, important in many fields, apart from the study of BECs: Non–linear optics, plasma physics, fluid dynamics, and spin–waves are a few examples [22, 23, 24, 25]. The ease with which the potential and non–linearity can be varied is one of the main appeals of BECs in the study of this equation.

An important set of solutions to the NLS equation are solitary waves, of the form $\psi(z,t) = \Phi(z-vt)\exp(i(kz-\omega t)$. There are two particularly important families: bright solitary waves and dark solitary waves. Bright solitary waves occur in the attractive case of negative g, and take the form of traveling, sech–shaped, density increases on zero background. Dark solitary waves occur in the repulsive case, and exist as traveling density depressions on a constant, non–zero, background [17]. In the literature, the term *soliton* is frequently used interchangeably with solitary wave in this context. Strictly, these solutions are not solitons, as they do not behave elastically in a collision (a defining property of a soliton) [26]. From this point onwards we will use the term soliton to describe these solitary waves, to remain consistent with the literature, and for brevity.

Recently, there has been an explosion of theoretical interest in *collisionally inhomogenous* environments [27, 28, 29, 30, 31, 32, 33], where g varies in space. This follows the experimental demonstration of such an environment in a Yb vapour [39]. The report to follow will focus on a 1D condensate, confined in 2D as explained above, where, in the unconfined direction, we introduce a square step/well in both V_{ext} and g (henceforth a *combined step*). The steps are chosen in a manner such that they allow a constant density ground state. The constant density constraint imposes a relationship between the step parameters; however, there is still some freedom in the form of the step. The report to follow will focus on the existence and stability of soliton solutions in this setting, specifically as the width of the step is varied. In the literature there have been many studies of spatially varying non–linearity (cited above), but far fewer looking at both non–linear and potential together, [34, §IV.B] provides a summary. The combined step setting we will investigate is interesting, as it allows us to examine the competition between the two effects (and their effects on the solution of the GP equation), whilst still being a relatively simple setting.

There are techniques in the literature for analysing the existence and stability of soliton solutions, summarised in [17]: these techniques are applicable in settings with either spatially varying non–linearities, external potentials, or both. I primarily used methods working from the non–linear limit, where we examine perturbations to a non–linear equation with a known set of solutions, in this case the NLS. The method I used involves forming an effective potential out of the perturbations to V_{ext} and g. Solitons exist at the extrema of this effective potential, their stability being determined by its curvature. The bright soliton case has been treated previously in this manner, with a different form of variation in the non–linearity and potential [36]. I took these results, and generalised the dark soliton methods in a similar manner. The repulsive case is complicated slightly by the need to adjust for the non–zero background density.

The report to follow will begin with a quick overview of the derivation of the GP equation and its validity. Following this, I will introduce the combined step setting more rigorously, before looking at what we might intuitively expect our results to be. Then, the theoretical tools needed to examine the effects of the step on soliton solutions will be introduced (section 2). These are the Bogoliubov-de Gennes (BdG) equations, which give the linear stability of the solutions; along with the effective potential theory discussed in the previous paragraph. We then move to numerical analysis to examine the validity of our theory (section3): solving the 1D GP equations for stationary solutions, and finding their stability eigenvalues by numerically solving the BdG equations. We follow this with a conclusion and suggestions for future work.

2 THEORY

2.1 Gross–Pitaevskii mean field theory

In this section we will follow through the derivation of the GP equation (more comprehensive treatments of the topic being found in any of [12, 17, 15, 16]), introducing the relevant physical quantities in more depth. We then derive the time-independent GP equation which will be im-

portant later in the report.

The derivation of the GP equation begins with the second quantised Hamiltonian of the full many body theory:

$$\hat{H} = \int d\mathbf{r}\hat{\Psi}^{\dagger}(\mathbf{r})\left[-\frac{\hbar}{2m}\nabla^2 + V_{\text{ext}}(\mathbf{r})\right]\hat{\Psi}(\mathbf{r}) \quad (2)$$
$$+ \frac{1}{2}\int d\mathbf{r}d\mathbf{r}'\hat{\Psi}^{\dagger}(\mathbf{r})\hat{\Psi}^{\dagger}(\mathbf{r}')V(\mathbf{r}-\mathbf{r}')'\hat{\Psi}(\mathbf{r}')\hat{\Psi}(\mathbf{r}),$$

where $\hat{\Psi}^{\dagger}$ and $\hat{\Psi}$ are the boson creation and annihilation operators at a point $\mathbf{r}$, $V(\mathbf{r}-\mathbf{r}')$ is the inter–atomic interaction potential, and V_{ext} is the external potential mentioned previously. The GP equation is a mean–field description of the above theory. Working now in the Heisenberg representation ($\hat{\Psi}$ is function of space and time), we replace the field operator in (2) by its expectation value, plus a small perturbation , $\hat{\Psi}(\mathbf{r},t) = \psi(\mathbf{r},t) + \hat{\Psi}'(\mathbf{r},t)$. The perturbation represents the non–condensate part of the gas [17, under eqn.(1)]. In a cold, dilute gas, we can replace the interaction potential, $V(\mathbf{r}-\mathbf{r}')$, by a delta–function potential of the form $g(\mathbf{r})\delta(\mathbf{r}-\mathbf{r}')$. The justification for this is that, in this regime, only low energy, two–body collisions are relevant, these are characterised by one physical parameter, the s–wave scattering length, a, independent of the details of $V(\mathbf{r}-\mathbf{r}')$ [12, 15, 16]. The s–wave scattering length is obtained by taking only the lowest order term in a partial–wave expansion (an expansion in terms of angular momentum eigenstates) of the two body scattering problem, and corresponds to low–energy isotropic scattering [35]. The s–wave scattering length is related to g by $g = 4\pi\hbar^2 a/m$: Positive g corresponds to repulsive interactions, negative g to attractive ones. Using the above approximations for $\hat{\Psi}$ and $V(\mathbf{r}-\mathbf{r}')$, together with the Heisenberg evolution equation for the field operator $\hat{\Psi}(\mathbf{r},t)$, gives the following mean–field equation for the order parameter,

$$i\hbar\frac{\partial}{\partial t}\psi(\mathbf{r},t) = \left(-\frac{\hbar^2\nabla^2}{2m} + V_{\text{ext}}(\mathbf{r}) + g|\psi|^2\right)\psi(\mathbf{r},t). \quad (3)$$

The first term is a kinetic term, the second is the external potential term, and the third is the non–linear term.

The validity of the dilute gas approximation (which allows us to make the replacement for $V(\mathbf{r}-\mathbf{r}')$ above) is dependent upon the smallness of the parameter $\langle n\rangle|a|^3$ [12, 17], where $\langle n\rangle$ is the average atomic density in the condensate. In typical experiments this parameter is always less than 10^{-3} [12]. The GP equation is strictly valid when $\hat{\Psi}' = 0$ and all the atoms are in the condensate, even at $T = 0$ correlation effects can lead to atoms leaving the condensate. Finite size effects can also come into play, as the number of atoms is not truly macroscopic. However, at low temperatures and with large numbers of atoms (but such that $\langle n\rangle|a|^3$ is still small), the GP equation provides a good description of experimentally observed behaviour. The GP equation can also be derived from the full many–body problem in a rigourous manner [14]

To reduce the GP equation to a 1D setting, as described in section 1, we use an harmonic trap to confine the condensate in two dimensions. The harmonic trap is described by, $V_{\text{ext}} = m/2((\omega_x x)^2 + (\omega_y y)^2 + (\omega_z z)^2)$, where $\omega_{x,y,z}$ are the *trapping frequencies* in each direction. We confine the condensate to the z axis, which becomes the axial direction. We now define the transverse oscillator frequency, $\omega_{\text{r}} \equiv \omega_x = \omega_y$. By using a highly anisotropic harmonic trap as the external potential, such that $\omega_{\text{r}} \gg \omega_z$, it is possible to reduce the full 3D theory to a quasi–1D one. The procedure for averaging over the transverse dimensions is detailed in [37]. The averaging is performed using a multi–scale technique which takes advantage of the disparate spatial scales in the two dimensions. The length scale associated with an harmonic trap is the *oscillator length*, $a_i = (\hbar/m\omega_i)^1/2$, which implies a ratio of length scales,$a_z/a_r = (\omega_r/\omega_z)^1/2$. A possible trapping ratio would be 5.6×10^4 [12, Fig. 7], giving $a_z/a_r = 236.6$. Performing the averaging gives the 1D GP equation. We use the rescaled variables $t' = t/\omega_r$, $z' = z/a_r$, and $|\psi'|^2 = |\psi|^2/2|a|$, to give the equation in dimensionless form:

$$i\frac{\partial}{\partial t}\psi(z,t) = \left(-\frac{1}{2}\frac{\partial^2}{\partial z^2} + V_{\text{ext}}(z) + g|\psi|^2\right)\psi(z,t), \quad (4)$$

where g is now rescaled to be ±1 for repulsive/attractive interactions[1]. For the rest of the report we will neglect the weak trapping in the z–direction, for simplicity.

[1]The rescaled variables are taken from [17], but have been altered for 1D, the paper uses a rescaled density appropriate for a 3D equation.

The GP equation can be reduced to a time–independent form by assuming a solution of the form $\psi(z,t) = \phi(z)e^{-i\mu t}$, substituting gives,

$$\left(-\frac{1}{2}\frac{\partial^2}{\partial z^2} - \mu + V_{\rm ext}(z) + g|\phi|^2\right)\phi(z) \;=\; 0. \quad (5)$$

The GP equation with a time–independent external potential has two conserved quantities associated with it: number of particles and energy [17, 12]. The number of particles, N, is given by $N = \int dz|\psi(z,t)|^2$ which implies that ϕ is normalised to the number of particles. The parameter μ is a dimensionless chemical potential, and is set to± 1 for the rest of the report: the positive sign corresponds to the repulsive case, the negative sign to the attractive one.

2.2 Non–linear and potential step with constant density solution

The scattering length, and hence the non–linearity, can be altered by a process known as Feshbach resonance management. In a collision process, the atoms involved will have spin structure. Zeeman splitting in the energy levels, as a result of the atomic spin, creates a number of channels (possible routes from input to final states) which the process can occur in. These channels can be divided into two types, open and closed channels. The result of the scattering process can only lead to atoms whose combined energy in their final states is less than the energy available, this is an open channel process. Closed channel processes are those with final states above the energy available, the scattering process cannot lead to atoms output into these final states. If the energy of a bound state of a closed channel is sufficiently close to the energy of the scattering state, this state can mix with the scattering state, leading to a modification of the scattering length. Varying the magnetic field near one of these resonances allows us to alter the energy separation of the channels, and hence allows us to tune the scattering length. We can now replace g in (5) with $g(z)$ [19].

To create a constant density situation, both within and external to the potential step, we work within the Thomas–Fermi (TF) approximation. The TF approximation consists of neglecting the second derivative term in the Hamiltonian, see [12], this is almost exact here due to the constant density nature of the ground state solution. The result is the following equation for the density in each region,

$$|\phi|^2 \;=\; g^{-1}(\mu - V_{\rm ext}),\; V_{\rm ext} < \mu. \quad (6)$$

If we then apply this to both regions, and equate the densities, we find that

$$g_1^{-1}(\mu - V_1) \;=\; g_2^{-1}(\mu - V_2), \quad (7)$$

where $g_{1,2}$ and $V_{1,2}$ are the non–linearity and potential in the two regions. It is possible for g_2 to differ from g_1, despite our rescaling, because the density is rescaled in terms of the scattering length outside the step. We now define $\gamma \equiv \Delta g/\Delta V = g_1/(V_1 - \mu)$, where $\Delta g = g_2 - g_1$, and similarly for ΔV. The step is determined fully by the parameter γ, together with $\Delta \equiv -\Delta V$ (this choice of Δ gives Δg with the same sign as Δ). Using γ as a parameter is useful, as it makes it clear that the relative sizes of Δg and ΔV are not independent. The step is now controlled by two parameters: the step width, defined as w, and the step height, Δ. Unless stated otherwise, for the numerical section of the report (section 3) we will take g_1 and V_1 to be given by their values in the non–linear limit (± 1 and 0), giving $\gamma = -1$. We will also impose a constraint on Δ, $|\Delta| < 1$, this prevents g from changing sign or becoming zero within the step region (this situation will be discussed in further work 4).

To avoid having non–smooth behaviour in our step, we will implement it as two tanh functions,

$$g \;=\; g_1 + \Delta g\left[\tanh(z_+) - \tanh(z_-)\right], \quad (8)$$
$$V \;=\; V_1 + \Delta V\left[\tanh(z_+) - \tanh(z_-)\right], \quad (9)$$

with $z_\pm = (z \pm z_w)/s$. This functional form gives a step with width $w = 2z_w$, with an edge region at z_w, whose width is characterised by s. The remainder of the report will primarily be an investigation of how the step width, w, affects the soliton solutions at various 'strengths', Δ. This is a particularly interesting situation when the width of the step becomes comparable with the width of the excitation. Using negative values for z_w in eqns (8,9) leads to the same step, but with the signs of Δg and ΔV swapped. Henceforth, we will keep Δ positive, using negative width to give negative Δg.

2.3 Soliton solutions to the GP equation

We begin to work towards our setting by first considering the type of solutions we would expect far from the step edges. If the solitons have velocity 0, the functional form of the soliton solutions are sech and tanh, for bright and dark solitons respectively [17]. The soliton solutions of the NLS can be generalised to include a constant V_{ext} and $g \neq \pm 1$ (my derivations are in appendix 3):

$$\phi_{\text{bs}}(z-\xi) = \sqrt{\frac{-2\omega_i}{-g_i}}\,\text{sech}(\sqrt{-2\omega_i}(z-\xi)), \quad (10)$$

$$\phi_{\text{ds}}(z-\xi) = \sqrt{\frac{\omega_i}{g_i}}\,\tanh(\sqrt{\omega_i}(z-\xi)), \quad (11)$$

with $\omega_i = \mu - V_i$. The parameter ξ is the solitons centre position. The constraint $|\Delta| < 1$ ensures that ω_i is the correct sign to give real roots above. The subscript, $i \in \{1, 2\}$, refers to different values of the constant potential/non–linearity, as defined in section 2.2. These soliton solutions are derived for an infinite domain, where we do not have a change in V_{ext} or g. The solution for $i = 1$ corresponds to no step. The solution for $i = 2$ corresponds to the limit of an infinitely wide step.

If we have a *wide*, finite, step in the equation, we expect the solution for $i = 1$ far outside the step. The solution for $i = 2$ is what we would expect near the centre of the step. We can see this by considering a soliton located at the origin, and introducing a wide step: the edges of this step would be located in a region of constant or zero density (as they are far outside the soliton), and thus the kinetic term in (5) will be zero, by relation (7), we know that the regions either side of the step allow the same density, thus, the solution is not altered by the introduction of a step.

The solitons (10,11) reduce to those given by the NLS for $i = 1$. When $i = 2$, the solitons differ from those which solve the NLS: the parameter governing the amplitude does not change (because of eqn. 7), however, the parameter governing the width does change. The soliton for $i = 2$ is wider than the standard NLS soliton when Δ is the opposite sign to μ, narrower when Δ has the same sign. When the step width becomes comparable to the width of the non–linear excitation, we can expect that the solution inside the step may be perturbed away from either of these limits.

2.4 Effective potential landscapes and stability analysis

The methods elucidated in the following sections are a powerful means of investigating the stability and persistence of soliton solutions to the GP equation when a perturbation is introduced. The combined step is introduced as a perturbation from the non–linear limit, characterised by a small parameter, ϵ. The procedure we will follow is similar to the analysis of equilibrium–points in ODE systems: finding an equilibrium–point, examining its stability by looking at small perturbations to this, and seeing how the stability alters as a parameter is varied. The PDE case is complicated in that we are instead looking for stationary solutions, rather than points, and seeing how perturbations to these solutions grow or decay [43]. We introduce a small perturbation to the excitation wave function we have found,

$$\begin{aligned}\psi(z,t) &= e^{-i\mu t}\Big[\phi(z) \\ &+ \sum_j (u_j(z)e^{-i\omega_j t} + v_j^*(z)e^{i\omega_j t})\Big], \quad (12)\end{aligned}$$

where $u_j(z), v_j^*(z), \omega_j \in \mathbb{C}$ are small, and describe the response to perturbations to ϕ oscillating at $\pm\omega_j$. Substituting (12) into the time–dependent GP equation, (4), and keeping only first order terms in the perturbation, we get the Bogoliubov–de Gennes equations [12, 17]:

$$\begin{aligned}Au_j(z) + Bv_j(z) &= \omega_j u_j(z), \\ Av_j(z) + B^* u_j(z) &= -\omega_j v_j(z), \quad (13)\end{aligned}$$

with

$$\begin{aligned}A &= -\frac{1}{2}\frac{\partial^2}{\partial z^2} + V_{\text{ext}} - \mu + 2g(z)|\phi|^2, \\ B &= g(z)\phi^2(z). \quad (14)\end{aligned}$$

The BdG equations can be used to assess the linear stability of any state ϕ. If an eigenfrequency, ω, solves the above, so also does $-\omega$ and $\pm\omega^*$. A purely imaginary doublet of eigenfrequencies leads to exponential growth of the relevant perturbation, and hence implies instability of that state along one eigendirection. A complex eigenfrequency quartet gives oscilllatory growth. Purely real eigenvalues imply the state is stable, the perturbations neither grow nor decay.

The eigenfrequency spectrum of the NLS is known for both bright and dark solitons. In the first case, there is a continuous spectrum of real eigenvalues above a certain minimum value, $\omega_{\min}$, below this value, there are four eigenvalues at the origin [48, Fig. 1]. In the latter case the spectrum fills the entire real axis, again, there is an eigenvalue with multiplicity 4 at the origin [49]. The eigenvalues at the origin are particularly important when considering perturbations from the non–linear limit, as they are related to the symmetries of the GP equation (4), namely phase invariance and translational invariance, which lead to its associated conservation laws[41]. When we break the translational invariance, by introducing the step, we cause the two eigenvalues associated with this symmetry to leave the origin[41]. When the eigenvalues leave the origin, they can move either along the imaginary axis, leading to instability, or along the real axis. When eigenvalues leave along the real axis they move away symmetrically in opposite directions. If a collision with a member of the continuous spectrum occurs, it can cause the eigenvalues to leave the axis as a complex eigenfrequency quartet [41, §7.0.2]. Leaving along the imaginary axis leads directly to instability.

We rewrite the GP equation in an appropriate form to consider perturbations to the potential and non–linearity characterised by ϵ,

$$i\psi_t = -\frac{1}{2}\psi_{zz} + (\epsilon n_1(z) + (g_1 + \epsilon n_2(z))|\psi|^2)\psi, \quad (15)$$

where we have used the subscripts to imply differentiation. The quantity ϵn_1 is the perturbation to V_1, $V - V_1$. The quantity ϵn_2 is the perturbation to g_1, $g - g_1$. The energy associated with the unperturbed part is [17],

$$E_0[\psi] = \frac{1}{2}\int_{-\infty}^{\infty}(|\psi_z|^2 + g_1|\psi|^4)dz. \quad (16)$$

The first term is the kinetic energy term, the second is due to the non–linearity, and hence interactions. Note the form of the non–linear energy term, dependent on the density squared.

We attempt to simplify our initially complicated problem by realising that we have identified a family of solutions to the NLS equation, characterised by their centre position. When we introduce the perturbation, ϵ, for certain centre positions there will exist what is called a continuation from the solution to the NLS equation, say $\phi_0(z-\xi_0)e^{-i\mu t}$, to the solution to the GP equation, $\phi_\epsilon(z-\xi_\epsilon)e^{-i\mu t}$: For certain centre positions, soliton solutions will still exist when the perturbation is introduced. To find the locations where these soliton solutions persist, we will follow the procedure outlined in [40, 41]. In [40, 41] we find that, intuitively, the locations where solitons persist are at the extrema of an energy functional for the perturbation. The stability of these solitons is related to the curvature of this energy functional. We will follow through the results for the dark soliton, these are complicated slightly by the presence of the background, which must be taken into account when we define our energy functional. The bright soliton result will merely be quoted, but is achieved in a similar way.

The results of [40] are derived for a potential which is bounded and decaying, these conditions are satisfied by our step. We will generalise the results, following [46, 41], to take into account a spatially varying nonlinear term, in addition to the potential term. In the repulsive case, our solution for the NLS, (11), satisfies the conditions given in [40, Main results, i]. Combining the result of [40], for an external potential, and [46], for a spatially varying nonlinearity, we find the following effective potential,

$$\begin{aligned} M'_{ds}(\xi_0) &= \int_{-\infty}^{\infty}\Big[n_1'(z)(\eta_{ds}^2 - \phi_0^2(z-\xi_0)) \\ &+ \frac{1}{2}n_2'(z)(\eta_{ds}^4 - \phi_0^4(z-\xi_0))\Big]dz = 0. \end{aligned} \quad (17)$$

The prime on $n_{1,2}$ implies derivative with respect to their argument, that on the M is merely notational. If 17 is fulfilled for some ξ_0, there exists a unique solution to the perturbed equation. This solution is $\phi_\epsilon(z-\xi_\epsilon)$, for ξ_ϵ ϵ–close to ξ_0, and is ϵ–close to $\phi_0(z-\xi_0)$ in the L^∞–norm[2]. The proof is quite involved,see [40, §2]: essentially, persistence of a solution upon introducing the perturbation is shown to be a result of the above condition (17), but for ϕ_ϵ rather than ϕ_0. The condition on ϕ_ϵ is less useful as the perturbed solutions are not known. The technique of Lyapunov–Schmidt reduction is used to prove that the above condition

[2] A measure of similarity between the functions. See [] for a definition

on ϕ_0 implies the condition on ϕ_ϵ, and hence that (17) implies persistence of solutions in the perturbed equation. Lyapunov–Schmidt reduction is a technique which allows us to reduce the problem from an infinite dimensional one, to one with a small number of parameters [42]. The problem is reduced to that of dealing with a bifurcation equation in few dimensions, in our case these are the parameters ϵ and ξ. The bifurcation equation can be solved and yields a correction to ϕ_0 that is unique, such that the corrected ϕ_0, ϕ_ϵ, satisfies the conditions mentioned below (17).

To analyse stability, it is necessary to look at,

$$\begin{aligned} M''_{ds}(\xi_0) &= \int_{-\infty}^{\infty}\Big[n''_1(z)(\eta_{ds}^2-\phi_0^2(z-\xi_0)) \\ &+ \frac{1}{2}n''_2(z)(\eta_{ds}^4-\phi_0^4(z-\xi_0))\Big]dz \neq 0, \end{aligned} \quad (18)$$

if $M''_{ds}(\xi_0) < 0$, the soliton is unstable with one imaginary eigenvalue; if $M''_{ds}(\xi_0) > 0$, the soliton is unstable with a pair of complex eigenvalues. These unstable eigenvalues appear as part of the other spectral structure described below equations (13,14). Given $M''_{ds}(\xi_0)$, it is possible to calculate an approximation to the eigenvalues for small ϵ:

$$O(\epsilon^2) = -\omega^2 + \frac{\epsilon}{4}M''_{ds}(\xi_0)\left(1-\frac{i\omega}{2}\right), \quad (19)$$

The root picked is that with $\mathrm{Real}(i\omega) > 0$ [40]. The above result verifies the assertion in the previous paragraph regarding stability, more importantly, it allows us to get a quantitative handle on the the eigenvalues.

In the attractive case, one determines stability in a similar manner, without having to worry about the background. The resulting equations for bright solitons are

$$\begin{aligned} M'_{bs}(\xi_0) &= \int_{-\infty}^{\infty}\Big[n'_1(z)\phi_0^2(z-\xi_0) \\ &+ \frac{1}{2}n'_2(z)\phi_0^4(z-\xi_0)\Big]dz = 0, \end{aligned} \quad (20)$$

with M''_{bs} being as above but with double primes within the integral. For the eigenvalues,

$$\omega^2 = \frac{\epsilon}{2\sqrt{-2\mu}}M''_{bs}(\xi_0) + O(\epsilon^2). \quad (21)$$

The simpler eigenvalue spectrum in the attractive case arises because the NLS spectrum does not include the origin, here the eigenvalues are imaginary, and hence unstable, for $M_b s''(\xi_0) < 0$ whilst being real, and hence stable, for $M_b s''(\xi_0) > 0$.

If, whilst varying a parameter, there is a sudden change in the qualitative nature of solutions (such as the number of solutions), as well as their stability, we say a *bifurcation* has occurred. We will find in the numerical sections of the report, 3, that our system exhibits a pitchfork bifurcation as the width of the step varies. Pitchfork bifurcations are common in physical systems [43] and are named for their shape, which resembles a pitchfork, they have a central branch which changes stability and two outer branches leaving the bifurcation point.

3 Numerical computations

We now build on our analytical results using numerical computations. To solve the time-independent GP equation, a Newton–Raphson iterative method is used. Given an initial guess which is sufficiently close to the initial solution, convergence is quick, around 5 iterations. The analytic solution to the NLS is a good place to start, as the soliton solution to the GP equation, if it exists, is usually of a similar form. The BdG equations are solved numerically by using a combination of MATLAB's `eig` and `eigs` commands on a discretised version of the equations, further details are in appendix B. Finally, to perform time–evolution simulations, we discretise the spatial part of the GP equation and use a fourth–order Runge–Kutta algorithmn to integrate in time. Finite difference methods are not the most appropriate for use with our equation, the NLS is better suited to split–step and fourier methods [44], they are, however, quick to program and easily adapted to a number of different situations: these are desirable traits given the length of time I had to approach the investigation.

3.1 Bifurcation diagrams

The functions $M'(\xi)$ and $M''(\xi)$ are easy to calculate numerically. Finding the zeros, $\{\xi_i\}$, of $M'(\xi)$, and the sign of $M''(\xi_i)$, allows us to find the points at which soliton solutions to the GP equation exist, along with their associated stability. We will look first at bright solitons, as they exhibit more interesting behaviour. We can simplify the equation for M' and M'' by realising the potential and non–linear step are just scaled ver-

sions of one another: if $n_1'(z) = \Delta n'(z)$, then $n_2'(z) = (\Delta/\gamma)n'(z)$ (see (8,9), n(z) is given by the tanh functions). We can now replace $n_{1,2}'$ and ϕ_0 in (20) and simplify,

$$\begin{aligned} M_{bs}'(\xi_0) &= \int_{-\infty}^{\infty}\Big[n_1'(z)\phi_0^2(z-\xi_0) \\ &+ \frac{1}{2}n_2'(z)\phi_0^4(z-\xi_0)\Big]dz = 0, \qquad (22) \\ &= \int_{-\infty}^{\infty} n'(z)m(z-\xi_0)dz, \qquad (23) \\ m(x) &\equiv \frac{2\Delta\mu}{g_1}(\mathrm{sech}^2\left(\sqrt{-2\mu}x\right) \\ &- \mathrm{sech}^4\left(\sqrt{-2\mu}x\right)). \qquad (24) \end{aligned}$$

Equation (24) defining $m(x)$ is interesting. Altering any of our parameters only scales $m(x)$ along one of the axes, it does not alter the functional form. The implication is that altering any of those parameters does not change the qualitative nature of the solutions, their number and stability for example, but only changes their centre positions by a scaling factor. The functional form of $n'(z)$ in (22) is aproximately two delta–functions, of opposite signs, at $\pm z_w$: the gradient of the functions describing the step, (8,9), is zero everywhere except at the step edges, where it is large. Substituting the delta–function form for $n'(z)$ in (22) gives $M'(\xi) = m(z_w - \xi) - m(-z_w - \xi)$, this form is shown in figure 1 for four step widths. Looking at the figure, we see that when the width becomes comparable to half of $m(z-\xi)$ the contributions from both sides of the step begin to overlap, this leads to more interesting structure arising.

I calculated the zeroes, $\{\xi_i\}$, of $M'(\xi)$ for step widths between -5 and 5. The set of points, $\{\xi_i\}$, correspond to the centres of solitons that have stability given by the sign of $M''(\xi_i)$. We can form a bifurcation diagram for the soliton centre positions by plotting the ξ_i against width, colouring the curves according to their stability. The result is figure 2. At very narrow step widths there are three zeros of $M'(\xi)$, these correspond to solitons centred at 0 or a little outside the step. The central soliton is of opposite stability to the external solitons. As the step widens, the central soliton solution changes stability in a pitchfork bifurcation, the external solitons also move outwards, but more slowly than the step widens, eventually meeting the outer branches of the pitchfork at the step edge. When the step is at its widest, the branch at the origin widens into a region about zero, solitons can exist at any point within this region. Tor both signs of Δ (positive and negative width on the diagram), the stability eigenvalues within the central region of solutions are vanishingly small: for unstable eigenvalues the instability development will be so prolonged that the solitons can be considered to be stable.

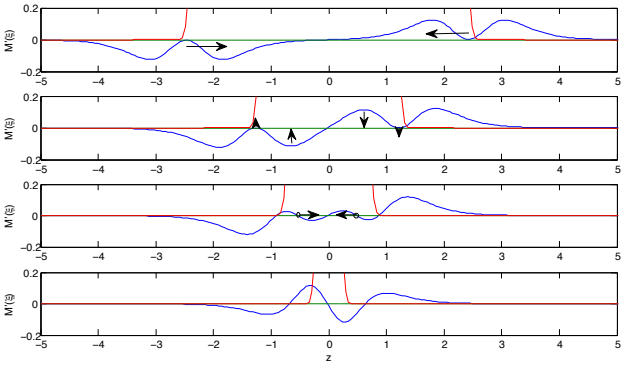

Figure 1: A diagram showing $M'(\xi)$ and how this evolves as the step (shown in red) narrows. The green line is at zero and helps pick out when $M'(\xi)$ touches/crosses the axis. The black arrows attempt to show the sequence of events described in the text. The interesting behaviour in this case is the formation of a further two fixed points which travel inwards to zero.

The positions of the outer soliton solutions at very narrow widths can be predicted by letting $n(z)$ tend to a delta–function. Substituting this into (23) and integrating by parts (to take care of the delta–function derivative) gives,

$$\begin{aligned} M'(\xi) &= -\int_{-\infty}^{\infty}\delta(z)m'(\sqrt{-2\mu}(z-\xi_0))dz, \\ m'(x) &= \frac{2\Delta\mu}{g_1}(-(\cosh(2x)-3)\tanh(x)\,\mathrm{sech}^4 \qquad (25) \end{aligned}$$

The zeros of $M'(\xi)$ are at 0 and ± 0.623. If we allow the newton raphson iterator to converge to a solution for very narrow widths (w = 0.1), we find solitons just outside the step are centered at ± 0.634, the prediction from the theory is correct to within 1.7%.

The discussion of this section has focused on the attractive case, the reason being that the qualitative nature of the solutions for dark solitons are much simpler: only the centre solution exists for dark solitons, and no bifurcations occur. The

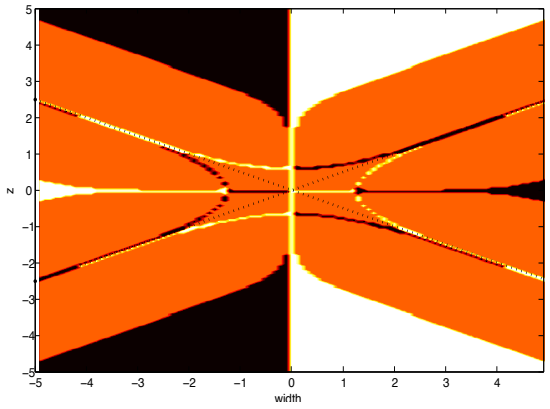

Figure 2: Bifurcation diagram for the bright soliton centre position, calculated for $\Delta = 0.1$. The orange regions do not admit soliton solutions, the light curves indicate the centre positions of unstable solitons, the dark curves stable ones. Outside the orange region, far from the step, the rest of the domain supports soliton solutions. The dotted lines indicate the step edge.

dark soliton branch at the origin is unstable for negative widths, oscillatory–unstable for positive widths: there is no change in stability as the step widens. Again, at very large widths the branch of solutions widens, becoming a region in which solutions can exist.

3.2 Soliton solutions and their stability

The previous section has confirmed the earlier intuitive arguments for wide steps (see section 2.3): soliton solutions exist, except within a narrow region about the step edge, in this region the solution is strongly perturbed. We have also revealed some interesting structure arising for narrow steps. To further investigate this behaviour we will use our Newton–Raphson iterative method to find solutions to the time–independent GP equation (5). Given there is always a branch of solutions at zero, we can apply a continuation type approach. Starting with a wide step, a soliton solution is allowed to converge to the correct solution. This new solution is then passed as the initial guess for the next width, in this manner, it is possible to get a set of solutions for all values of the width, more sophisticated methods are given in [45]. The BdG equations (13,14) are solved numerically to give the associated stability eigenvalues for each solution, these are compared with those given by the theory of section 2

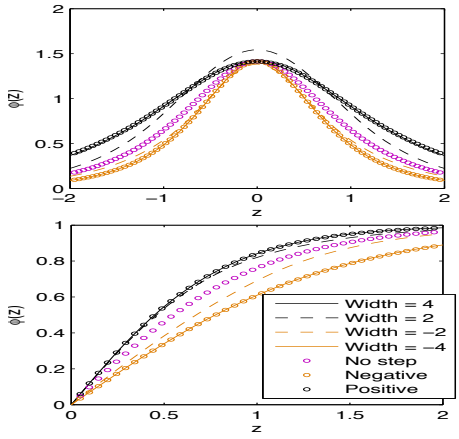

Figure 3: Soliton solutions centred at zero for attractive (top) and repulsive (bottom) interactions. The legend holds for both sets of solutions. The solid line solution is barely visible in both cases, as it is overlapped by positive/negative.

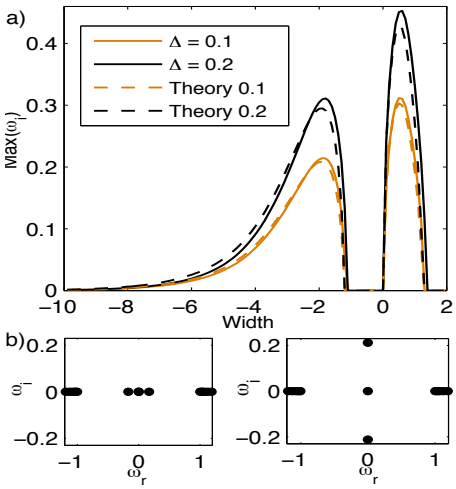

Figure 4: a) Max imaginary part of eigenvalues against width. b) Typical eigenvalue development in unstable (top) and stable (bottom) regions.

Figure 3 shows the soliton solutions for a variety of widths, in both attractive and repulsive cases. The curves labelled positive and negative correspond to the solitons (10,11) with $i = 2$, where positive and negative refer to $\omega_2 = \mu \pm \Delta$. It can be seen that these are the limiting forms of the solitons centred at zero for wide steps. As the step narrows, the solitons become different from these limiting forms, but do not tend to the solution in the absence of the step. Instead, the solitons narrow and grow in amplitude, for positive width; widen and shrink, for negative. The opposite occurs for dark solitons, but with no change in amplitude.

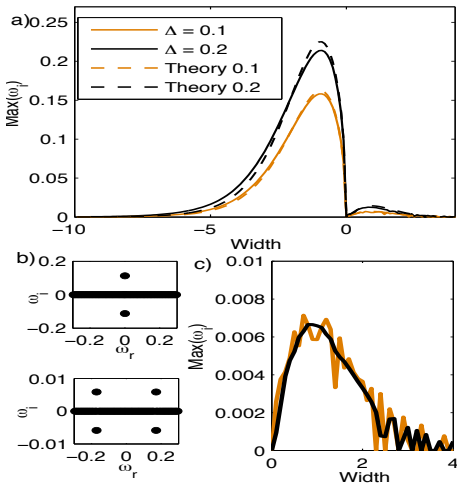

Figure 5: a) Max imaginary part of eigenvalues against width. b) Typical eigenvalue development in unstable (top) and oscillatory–unstable (bottom) regions. c) How domain size affects the numerical simulation: black being large domain, orange small.

Figure 4a) compares numerical and theoretical (dashed) values for the imaginary part of the eigenvalues against width. The previously identified bifurcations are clearly visible as sudden large increases in the magnitude of the stability eigenvalue. The theory predicts the eigenvalues very well, except very near the bifurcation. As the perturbation size is increased it can be seen that the numerical values are less well described quantitatively, however qualitative agreement is still good. For both strengths the theoretical predictions are within ϵ of the numerical values, usually well within this region. With growing perturbation strength the size of the instability also grows. The insets show the translational eienvalues leaving the origin, along either the real or imaginary axis. When the eigenvalues move along the real axis, they do not enter the continuous spectrum and hence cannot lead to oscillatory instability through collision (see section 2.4).

Figure 5a), shows the dark soliton case. Notable differences are the immediate instability at zero width, the solutions being either unstable, or oscillatory–unstable, for all widths. As mentioned in section 2, this is a result of the eigenvalue spectrum encompassing the origin. Figures 5b) show typical eigenvalue development. Note the eigenvalue quartet which results in oscillatory instability. Also noticable in the subfigures is the lack of a gap about the origin, this is markedly different

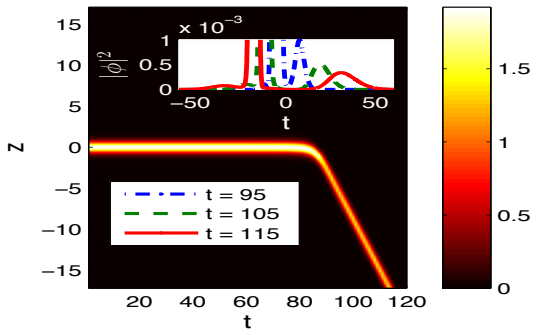

Figure 6: Main figure: unstable soliton leaving the step. Inset: snapshots of the density at 3 times. Both the counter propagating dispersive wave, and that infront of the soliton are clearly visible. Parameters: $\Delta = 0.5$ with width of -2.

to the bright soliton case (see figure 4b)). Figure 5c) shows an interesting numerical effect: simulating the infinite domain on a finite numerical one (which cannot be avoided) causes the continuous eigenvalue spectrum to become discrete, a result of this is that occassionally the oscillatory eigenvalues 'drop' back to the real axis when they encounter a gap in the spectrum [], this leads to the 'spikes' shown. The behaviour we see does not reflect the actual physical situation, where the eigenvalues should be a quartet with non–zero imaginary part throughout the region. The subfigure demonstrates how the effect lessens with increased domain size, where the gaps in the spectrum become smaller.

In order to study the development of instabilities, we use the Runge–Kutta integrator. The initial input for the integrator is a solution given by the Newton–Raphson method. In both cases unstable solitons move off from the origin after an amount of time dictated by the strength of the instability. As the soliton leaves the step it emits two dispersive waves: one travels ahead, one is counter–propagating behind the soliton. Number is still conserved, with the soliton decreasing in amplitude. These dispersive waves are mentioned in [46, 47], which both cover piecewise constant periodic potentials, external and non–linear respectively, where the soliton dissipates constantly to zero. The emission of dispersive waves is a result of the soliton moving over a spatially inhomogeneous environment, and hence is concentrated at the step edges. As a result, in our setting the emission of a wave occurs only once, when leav-

ing the step, and the soliton is persistent despite its initial instability. The case shown is that of a bright soliton, dark solitons behave similarly.

4 Conclusion

I investigated a combined nonlinear and external–potential step in the 1D GP equation, arranged to give a constant density ground state. Due to the simplicity of the setting, it was possible to investigate how the two effects compete or combine in a clear way, and the result on soliton solutions to the GP equation and their stability. I began by introducing the soliton solutions to the GP equation, generalising them to take into account the presence of a constant potential and nonlinearity. Doing so allowed us to consider the forms of the soliton solutions far from the edges of the step. I picked the width as a step parameter to focus on, being interested in the behaviour of the solution when the step became of similar width to the nonlinear excitations. I then introduced various theoretical and numerical tools to investigate the kinds of solutions supported and their stability.

A theoretical framework was introduced, which aimed to explain the existence and linear stability of soliton solutions via an effective potential landscape. Solitons persist at the extrema of this potential landscape, with stability governed by whether they exist at maxima, or minima, of said potential. I generalised previous results to apply to a combined step setting. The linear stability was given quantitatively by the BdG equations for the stability eigenvalues, which describe how perturbations to solutions grow or decay. It was found that changing the parameters of the step has little effect on the qualitative nature of the solutions, only altering the magnitude of the stability eigenvalues, and shifting the centre positions of solitons solutions. Bright solitons were found to exhibit more interesting behaviour as the width was varied. A pitchfork bifurcation occurs at narrow widths, as the width increases the outer branches tend to towards two further branches of solutions at the edges of the step. Dark solitons exhibit less interesting behaviour, having only one branch of soliton solutions. The dark solitons are unstable for negative width, oscillatory–unstable for postive width.

We then moved to numerical studies to investigate the nature of the soliton solutions supported in more depth. For wide steps the solitons supported are those given by the limit of an infinitely wide step, as the step narrows the solitons alter. Calculation of the stability eigenvalues, by numerically solving the BdG equations, leads to eigenvalues in very good agreement with those given by the effective potential theory. In the limit of very wide steps, solitons centred at the origin, or in a region well within the step, are either stable or unstable with exponentially small eigenvalue. As the step narrows towards the point where the bifurcation occurs the eigenvalue grows in magnitude, before changing stability at the bifurcation point. The typical development of instability was then shown, the soliton eventually becomes mobile, leaving the step and emitting dispersive waves.

There are several avenues to pursue in further study, remaining with our setting in one–dimension, moving to higher dimensions or moving towards a more experimentally feasible setup. One way forward, is to investigate the relationship between narrow step states and defect–modes, which are solutions supported by a delta–function potential/non–linearity. At narrow step widths, the form (8,9) for the potential does not adequately represent the step. The limit of narrow width should be a delta–function, in my setting the tanh functions overlap, leading to the step eventually vanishing. It would be interesting to simulate the very narrow step properly, and investigate how the states supported by a delta–function relate to the solitons supported by narrow steps. A second way forward would be to investigate the solutions in the case where the nonlinearity changes sign within the step, this may have an interesting effect on the edge states as presumably the soliton centred at zero would no longer be supported. It would also be interesting to look at the setting either in higher dimensions, where other types of solutions such as vortices are supported, or to use a better one–dimensional reduction such as [50].

5 Acknowledgments

I would like to thank my supervisor, Mason Porter, for his suggestions and help along the way.

References

[1] Bose S N 1924 *Z. Phys.* **26** 178

[2] Einstein A 1924 *Sitzungsber. K. Preuss. Akad. Wiss., Phys. Math. Kl.* **261**
Einstein A 1925 *Sitzungsber. K. Preuss. Akad. Wiss., Phys. Math. Kl.* **3**

[3] London F 1950 *Superfluids* (New York : Wiley ; London : Chapman and Hall)

[4] Bardeen J, Cooper L N, and Schrieffer J R 1957 *Phys. Rev.* **108**, 11751204

[5] Anderson M H, Ensher J R, Matthews M R, Wieman C E, and Cornell E A 1995 *Science* **269** 5221

[6] Davis K B, Mewes M O, Andrews M R, van Druten N J, Durfee D S, Kurn D M, and Ketterle W 1995 *Phys. Rev. Lett.* **75** 3969

[7] Bradley C C, Sackett C A, Tollett J J, and Hulet R G 1995 *Phys. Rev. Lett.* **75** 1687

[8] Weber T, Herbig J, Mark M, Ngerl H, and Grimm R 2003 *Science* **299** 5604

[9] Modugno G, Ferrari G, Roati G, Brecha R J, Simoni A, and Inguscio M 2001 *Science* **294** 5545

[10] Takahashi Y, Takasu Y, Maki K, Komori K, Takano T, Honda K, Yamaguchi A, Kato Y, Mizoguchi M, Kumakura M, and Yabuzaki T 2004 *Laser Physics* **14** 4

[11] Griesmaier A, Werner A J, Hensler S, Stuhler J, and Pfau T 2005 *Phys. Rev. Lett.* **94** 160401

[12] Dalfovo F, Giorgini S, Pitaevskii L P, and Stringari S 1999 *Rev. Mod. Phys.* **71** 463512

[13] Bongs K and Sengstock K 2004 *Rep. Prog. Phys.* **67** 907

[14] Lieb E H, Seiringer R, Solovej J P, and Yngvason J *arXiv:cond-mat* 0610117v1

[15] Pitaevskii Stringari

[16] Pethick C and Smith

[17] Carretero-Gonzalez R,Frantzeskakis and Kevrekidis P G 2008 *Nonlinearity* **21** R139–R202

[18] Fortgh J and Zimmermann C 2005 *Science* **307** 860

[19] Chin C, Grimm R, Julienne P, and Tiesinga E 2010*Rev. Mod. Phys.* **82** 1225

[20] Inouye S, Andrews M R, Stenger J, Miesner H -J, Stamper-Kurn D M, and Ketterle W 1998 *Nature* **392** 151154.

[21] Theis M, Thalhammer G, Winkler K, Hellwig M, Ruff G, Grimm R, and Hecker Denschlag J 2004 *Phys. Rev. Lett.* **93** 123001

[22] Porter M A, Centurion M, Pu Y, Kevrekidis P G, Frantezeskakis D J, and Psaltis D *Proc. Appl. Math. Mech.* **7** 20300292030030

[23] Haas F and Shukla P K 2009 *Phys. Rev.* E **79** 066402

[24] Stancil DD and Prabhakar A 2009 *Spin Waves: Theory and Applications* Springer Science

[25] Ablowitz M J 2011 *Nonlinear Dispersive Waves: Asymptotic Analysis and Solitons* Cambridge University Press

[26] Zabusky N J, Porter M A 2010 *Scholarpedia* 5(8) 2068.

[27] Abdullaev F Kh and Garnier J 2005 *Phys. Rev.* A **72** 061605

[28] Sakaguchi H and Malomed B A 2006 *Phys. Rev.* E **73** 026601

[29] Abdullaev F Kh, Gammal A, and Tomio L 2004 *J. Phys. B* **37** 635

[30] Carpentier A V, Michinel H, Rodas–Verde M I, Prez-Garca V M 2006 *Phys. Rev.* A **74** 013619

[31] Theocharis G, Schmelcher P, Kevrekidis P G, and Frantzeskakis D J 2006 *Phys. Rev.* A **74** 053614

[32] Bludov Y V, Brazhnyi V A, and Konotop V V 2007 *Phys. Rev.* A **76** 023603

[33] Niarchou P, Theocharis G, Kevrekidis P G, Schmelcher P, and Frantzeskakis D J 2007 *Phys. Rev.* A **76** 023615

[34] Kartashov Y V, Malomed B A, and Torner L 2011 *Rev. Mod. Phys.* **83** 247305

[35] Landau L D and Lifshitz E M *Quantum Mechanics: Non-relativistic Theory*

[36] Rapti Z, Kevrekidis P G, Konotop V V, and Jones C K R T 2007 *J. Phys. A: Math. Theor.* **40** 14151

[37] Perez-Garcia V M, Michinel H, and Herrero H 1998 *Phys. Rev.* A **57** 3837

[38] Ablowitz M, and Prinari B 2008 *Scholarpedia* 3(8):5561

[39] Yamazaki R, Taie S, Sugawa S, and Takahashi Y 2010 *Phys. Rev. Lett.* **105** 050405

[40] Pelinovsky D E, and Kevrekidis P G 2008

[41] Kapitula T, Kevrekidis P G, and Stanstede B 2005 *Physica* D **201** 199

[42] Golubitsky M and Schaeffer D G 1985 *Singularities and Groups in Bifurcation Theory, Vol. I* (New York : Springer-Verlag)

[43] Cross M C and Hohenberg P C 1993 *Rev. Mod. Phys.* **65** 3

[44] Taha T R and Ablowitz M J 1984 *J. Comp. Phys.* **55** 2

[45] Allgower E L, Georg K 2003*Introduction to Numerical Continuation Methods* (New York : Wiley)

[46] Rodrigues A S, Kevrekidis P G, Porter M A, Frantzeskakis D J, Schmelcher P, and Bishop A R 2008 *Phys. Rev.* A **78** 013611

[47] Parker N G, Proukakis N P, Barenghi C F, and Adams C S 2004 *J. Phys. B* **37** S175

[48] Kapitula T and Sandstede B 1998 *Physica* D **124** 58-103

[49] Kapitula T and Rubin J 2000 *Nonlinearity* **13** 77112

[50] Salasnich L 2009 *J. Phys.* A *Math. Theor.* **42** 335205

A Analytics

Here I derive the form of bright and dark solitons in the GP equation with constant external potential, V, and a constant nonlinearity, g. The derivation begins with the time–independent GP equation:

$$\left(-\frac{1}{2}\frac{\partial^2}{\partial z^2} - \mu + V + g|\phi(z)|^2\right)\phi(z) \;=\; 0. \tag{26}$$

The soliton solutions to the NLS are,

$$\phi_{\rm bs}(z-\xi) = \sqrt{-2\mu}\,{\rm sech}(\sqrt{-2\mu}(z-\xi)), \tag{27}$$

and,

$$\phi_{\rm ds}(z-\xi) = \sqrt{\mu}\tanh(\sqrt{\mu}(z-\xi)), \tag{28}$$

where μ is -1 for bright solitons, and $+1$ for dark solitons. The soliton solutions with constant V and g can be expected to be similar to those of the NLS, with a new chemical potential $\omega = \mu - V$, and different constants within and without the sech function.

A.1 Bright soliton

We insert the ansatz,

$$\phi_{\rm bs}(z) = a\,{\rm sech}(bz), \tag{29}$$

into (26) giving,

$$-\frac{1}{4}ab^2(2\cosh^2(bz) - 4)\,{\rm sech}^3(bz) \;=\; a(\omega - ga^2\,{\rm sech}^2(bz))\,{\rm sech}(bz) \tag{30}$$

$$-\frac{b^2}{2} + b^2\,{\rm sech}^2(bz) \;=\; \omega - ga^2\,{\rm sech}^2(bz). \tag{31}$$

Comparing the coefficients in (31) gives $b = \sqrt{-2\omega}$ and $a = b/\sqrt{-g}$. The final result is (10).

A.2 Dark soliton

We insert the ansatz

$$\phi_{\rm ds}(z) = a\tanh(bz)), \tag{32}$$

into (26) giving,

$$-\frac{1}{2}(-2ab^2(1-\tanh^2(bz))\tanh(bz) \;=\; a(-\omega + ga^2\tanh^2 bz)\tanh(bz) \tag{33}$$

$$b^2 - b^2\tanh^2(bz) \;=\; \omega - ga^2\tanh^2(bz). \tag{34}$$

Comparing the coefficients in (34) gives $b = \sqrt{\omega}$ and $a = b/\sqrt{g}$. The final result is (11).

Appendix B.1

```
function [initial_phi,E_val,E_the,E_vec,E_con,V,g,x,store,n,dom,width] = GP_statR(u_guess,x0,type)

\%Takes a u_guess for continuation, if this is not required
input 1.  The other input is either 'b' or 'd' and selects bright or dark soliton versions.
initial_phi is the output, E_val is the eigenvalue spectrum, E_the is the theoretical eigenvalue
spectrum,
E_vec is a matrix of eigenvectors, E_con is a check variable for eigenvalue convergence.
The remaining parameters specify the step.\%

switch type
    case 'b'
        load('stat_par_bright.mat');
    case 'd'
        load('stat_par_dark.mat');
    otherwise
        disp('No File');
end

\%The above are two files of parameters\%

n =     stat_par(1);
dom =   stat_par(2);

\%Takes the number of lattice points and the domain size from
the parameter file\%

dx = dom/n;
x_min = -(dom/2);
x_max = (dom/2)-dx;
x = x_min:dx:x_max;
x = x';

\%Creates an x vector\%

g1      =  stat_par(3);
dg      =  stat_par(4);
V1      =  stat_par(5);
mu      =  stat_par(6);
width   =  stat_par(7);
sharp   =  stat_par(8);
win     =  stat_par(9);

\%Takes parameters from the parameter vector and converts them to separate
variables for easier later use. The parameters are the nonlinearity outside
the step, the change in nonlinearity (also Delta), the external potential
outside the step, the chemical potential, the width of the step, the width
of sloped part of the tanh (how sharp the step is), and a parameter for
eigenvalue finding.\%

R = (V1 - mu)/g1;

\%Calculates the Vext/non-linearity ratio.\%

dV = R * dg;

V2 = V1 + dV;



g_width = width/2;
g_sharp = sharp;

V_width = width/2;
V_sharp = sharp;

g = g1 + (dg/2)*(tanh((x + g_width)/g_sharp)-tanh((x - g_width)/g_sharp));

V = V1 + (dV/2)*(tanh((x + V_width)/V_sharp)-tanh((x - V_width)/V_sharp));

\%Forms the nonlinear and external potential steps.\%

if u_guess == 1
```

```
   u_guess = (sqrt(-2*(mu)))*sech(sqrt(-2*(mu))*(x-x0));
elseif u_guess == -1
    u_guess = (sqrt(mu))*tanh(sqrt(mu)*(x-x0));
end

\%Provides input if no initial function is passed.\%

v_guess = zeros(n,1);

\%Sets the imaginary part of the input to zero.\%

g = [g;g];
V = [V;V];
w = [u_guess;v_guess];

\%Manipulates g,V,u_guess and v_guess into a form that will be required later.\%

D = sparse(1:n,1:n,-2*ones(1,n),n,n);
E = sparse(2:n,1:n-1,ones(1,n-1),n,n);
L = (E+D+E')./(dx^2);
L2 = L + ( sparse([1 n], [1 n], [1 1],n,n) )./(dx^2);

\% Define the finite difference matrix
with boundary conditions that the first derivative
is 0 at boundary of domain (ie x -> infinity).\%

lim = 10;
k = 1;

\%Set initial values to be used in the iteration to follow.\%

while lim > 1e-9

    \%Iteration runs until the RHS of the TIGP equation is 1e-9.\%

    if type == 'b'

        w(1) = 0;
        w(n) = 0;

    elseif type == 'd'

        w(1) = -sqrt(mu - V1);
        w(n) = +sqrt(mu - V1);

    end

    \%Further BC's on solution. The wavefunction is ~ zero as x -> infinity
for bright solitons. For dark solitons the solution tends to some background
as given above.\%

    J = jacob(w,mu,V,g,dx,n);

    \%Calculates the Jacobian.\%

    F = GP(w,mu,V,g,L2,n);

    \%Finds the value of the GP equation LHS with w(n).\%

    delta = J\F;

    F2 = GP(w-delta,mu,V,g,L2,n);

    \%Finds the value of the GP equation LHS with w(n+1).\%

    w = w - delta;

    \%Iterates w(n) to w(n+1)\%

    lim = max(abs(F2))

    \%Checks the size of the LHS of the GP equation post iteration, this
is tested against the criterion lim>1e-9
```

```
    store(:,k) = w(1:n);

    \%Stores values of u throughout in order to examine convergence.\%

    k = k +1;

    \% Increments a counter to show number of iterations.  Also useful if
     need to stop iterating before convergence (ie if solution doesn't
     converge and you want to examine behaviour, set a maximum k).\%

end

u = w(1:n);
v = w(n+1:2*n);

V = V(1:n);
g = g(1:n);

phi0 = u + 1i*v;

\%Creates the output by conbining real and imaginary parts of phi_0.  Also
takes V and g back to their original forms.\%

[E_val,E_vec,E_con] = BdG(phi0,g,V,n,mu,L2,dx,win,type);

\%Calculates the eigenvalues and eigenvectors of the stationary solution in
the BdG equations.  Also outputs a check on convergence\%

E_the = eig_pred(g,V,mu,dx,L,x,type,g1);

\%Calculates the theoretical values of the eigenvalues.

initial_phi = phi0;


function J = jacob(w,mu,V,g,dx,n)

\%The function below calculates the jacobian of F, the program only puts variables
into a previously worked out Jacobian, it does not differentiate etc.\%

u = w(1:n);
v = w(n+1:2*n);
u2= [u;u];
v2= [v;v];

A = (1/dx^2 - mu) + V + g.*((u2.^2 + v2.^2)+(2*w.^2));
A(1) = A(1) -1/(2*dx^2);
A(n) = A(n) -1/(2*dx^2);
A(n+1) = A(n+1) -1/(2*dx^2);
A(2*n) = A(2*n) -1/(2*dx^2);

B = [0;(-1/(2*dx^2))*ones(n-1,1);0;(-1/(2*dx^2))*ones(n-1,1)];

C = [zeros(n,1);2*g(1:n).*u.*v];

J = spdiags([B C], [1 n],2*n,2*n);
J = J + J';
J = J + spdiags(A,0,2*n,2*n);



function F = GP(w,mu,V,g,L2,n)

\%The function below calculates the value of the LHS of the GP equation with our
present initial solution\%

u = w(1:n);
v = w(n+1:2*n);
u2= [u;u];
v2= [v;v];

L22 = [L2 0*L2;0*L2 L2];

F = -0.5*L22*w - mu*w + V.*w + g.*(u2.^2 + v2.^2).*w;
```

```
function [E_val,E_vec,E_con] = BdG(initial,g,V,n,mu,L2,dx,win,type)

\%For bright solitons computational time is saved by calculating the eigenvalues on
a restricted domain, this does not affect the results, so long as the domain is
sufficiently larger than the step region.\%

if type == 'b'

p_window = win;
p_max = n/2 + floor(p_window/dx);
p_min = n/2 - floor(p_window/dx);
phi0 = initial(p_min:p_max);
p_num = p_max - p_min + 1;



V=V(p_min:p_max);
g=g(p_min:p_max);

\%Restrict the part of the the stationary solution to be analysed in order
to reduce computational complexity.\%

a1 = V + 2*g.*(abs(phi0).^2) - mu*ones(p_num,1);
b1 = g .* (phi0 .^ 2);
b2 = g .* (conj(phi0) .^ 2);
b = spdiags(b1,0,p_num,p_num);
bc= -spdiags(b2,0,p_num,p_num);
a = (-0.5*L2(p_min:p_max,p_min:p_max)) + spdiags(a1,0,p_num,p_num);

A = [a,b;bc,-a];

\%Form a finite-difference version of the BdG equations.

[E_vec,E] = eig(full(A));

\%Finds the eigenvalue of the discretised BdG equations

C = A*E_vec - E_vec*E;
C = max(C);

E_con = C';

\%E_con is a check on eigenvalue accuracy.\%

E_val = diag(E,0);

elseif type == 'd'

 phi0 = initial;

\%For dark solitons reducing the computational domain adversely affects results.
Instead we use eigs, which is appropriate for large sparse matrices.\%

a1 = V + 2*g.*(abs(phi0).^2) - mu*ones(n,1);
b1 = g .* (phi0 .^ 2);
b2 = g .* (conj(phi0) .^ 2);
b = spdiags(b1,0,n,n);
bc= -spdiags(b2,0,n,n);
a = (-0.5*L2) + spdiags(a1,0,n,n);
A = [a,b;bc,-a];

\%Form a finite-difference version of the BdG equations.\%

[E_vec,E] = eigs(A,175,0.01);

\%Finds the 175 smallest eigenvalues of the discretised BdG equations.\%

C = A*E_vec - E_vec*E;
C = max(C);

E_con = C';
```

```
\%E_con is a check on eigenvalue accuracy.\%


E_val = diag(E,0);

end


function [P] = eig_pred(g,V,mu,dx,L,x,type,g1)

\%Numerically calculates the values of M''(x) and uses this to calculate theoretical
values for the eigenvalues.\%

if type == 'b'
initial = sqrt((-2*mu)/-g1)*sech(sqrt(-2*mu)*x);
    disp('moose')
n1 = - 1*(g-g1);
n2 = V;

S = 0.5*(L*n2).*((initial).^2) - 0.25*(L*n1).*((initial).^4);

S = (-1/sqrt(-2*mu))*sum(S).*dx;
P(1) =  sqrt(S);
P(2) = -sqrt(S);

elseif type == 'd'
    initial = sqrt(mu/g1)*tanh(sqrt(mu)*x);

    n1 = g - g1;
    n2 = V;

    S = L*n2 .* (mu^2 - initial.^2) + 0.5*L*n1 .* (mu^4 - initial.^4);
    S = (1/16)*sum(S).*dx;

    P(1) = S*(1+sqrt(1-4/S));
    P(2) = S*(1-sqrt(1-4/S));

end
```

Appendix B.2

```
function [mod_u_plot] = soliton_gW(n,dom,t,tf,u,g,V,mu,width)

\%Function to calculate evolution of an initial u, also specify all
parameters such that input can come directly from the stationary solutions
finder (Newton-Raphson). tf allows correction to the time step for larger domains,
such the the RK4 algorithm converges dt must be less than ~ dx squared\%

tic
dx = dom/n;
x_min = -(dom/2);
x_max = (dom/2)-dx;
x = x_min:dx:x_max;
n = numel(x);
x = x';

\%Define x grid

D = sparse(1:n,1:n,-2*ones(1,n),n,n);
E = sparse(2:n,1:n-1,ones(1,n-1),n,n);
S = E+D+E';
F = sparse([1 n],[1 n],[1 1],n,n);

\%Define the finite difference matrix with Dirichlet BCs\%

L2 = S +  F;
L2 = L2./(dx^2)



\% Set up variables to count etc and preallocate storage matrix.  dt is
timestep, kk is a counting value, t is the time solved until. dt_disp is
determines when values are taken to plot.\%



dt = (1e-3)/tf;
kk = 1;

t_max = t/dt
dt_disp = (1)/dt

initial_width = size(u,1);
initial_h = int32(t_max/dt_disp);

um = zeros(initial_width,initial_h);

\%Initialise waitbar to provide indication of progress through computation.\%

l = waitbar(0,'Computation in progress...');


\%Run main for loop for computation.\%

tic

for m = 1:t_max

    \%Runge-Kutta on u to get u at t + dt, the if statement takes values
    every 10 timesteps to output.\%

    u = rk4(u,x,dt,V,g,L2,m);

    if mod(m-1,dt_disp)==0

        um(:,kk) = u;
        kk = kk+1

    end

    \%Update waitbar.\%
    frac = m/t_max;
    waitbar(frac)
```

```
end

close(l)
toc

\%Outputs mod square of u for plotting at times t and points x.\%

mod_u = abs(um).^2;

\%Checks that number is conserved\%

number = sum(abs(um(:,1:kk-1)).^2)*dx;

figure
plot(number);
toc
number(end)-number(1)
mod_u_plot = mod_u;


\%Function to compute u at time m+1, given u at time m, the time and space
steps, along with initial u at time m.\%

function utdt = rk4(ut1,x,dt,V,g,L,m)

t = (m)*dt;

k1 = dt*finitedifference(ut1,x,V,g,L,t);
ut2 = ut1 + 0.5*k1;
k2 = dt*finitedifference(ut2,x,V,g,L,t+0.5*dt);
ut3 = ut1 + 0.5*k2;
k3 = dt*finitedifference(ut3,x,V,g,L,t+0.5*dt);
ut4 = ut1 + k3;
k4 = dt*finitedifference(ut4,x,V,g,L,t+dt);

utdt = ut1 + (1/6)*(k1+ (2*k2) + (2*k3) + k4);



\%Takes a given u and works out the finite difference at spatial lattice
points. Outputs this as f.\%

function f = finitedifference(u,x,V,g,L,t)

f= -1i*((-0.5).*(L)*u + V.*u + (g).*(abs(u).^2).*u);
```